Advances in Applied Mathematics and Mechanics
Adv. Appl. Math. Mech., Vol. 7, No. 6, pp. 780-795

DOI: 10.4208/aamm.2014.m627
December 2015

Fracture Analysis in Orthotropic Thermoelasticity Using Extended Finite Element Method

Honggang Jia[1] and Yufeng Nie[1,*] and Junlin Li[2]

[1] *Department of Applied Mathematics, School of Science, Northwestern Polytechnical University, Xi'an 710129, China*
[2] *Taiyuan University of Science and Technology, School of Applied Science, Taiyuan 030024, China*

Received 20 May 2014; Accepted (in revised version) 25 November 2014

Abstract. In this paper, a method for extracting stress intensity factors (SIFs) in orthotropic thermoelasticity fracture by the extended finite element method (XFEM) and interaction integral method is present. The proposed method is utilized in linear elastic crack problems. The numerical results of the SIFs are presented and compared with those obtained using boundary element method (BEM). The good accordance among these two methods proves the applicability of the proposed approach and conforms its capability of efficiently extracting thermoelasticity fracture parameters in orthotropic material.

AMS subject classifications: 65M60, 74A45

Key words: Fracture, orthotropic, thermoelasticity, interaction integral method, XFEM.

1 Introduction

Recently, growing focus on orthotropic materials used in aerospace and automobile industries, temperature field problem may be involved in the engineer component, hence, studying thermal fracture in these elastic materials has been among the most interesting topics of research in recent decades. For simple and special geometry [1] problem, the analytic or semi-analytic method is frequently used. However, for general or complex geometries problem, numerical method is an advisable choice. The existing numerical methods such as finite element method whose meshes assignment require been conformed to the discontinuities or singular singularity. To overcome the difficulties, XFEM [2,3] has been proven to be an efficient method for discontinuities problems which

*Corresponding author.
Email: yfnie@nwpu.edu.cn (Y. F. Nie), z770428@126.com (H. G. Jia)

does not need remeshing in the process of crack growth. For thermoelastic fracture problems using XFEM, thermal problems in [4–6] were involved to solve shear band problems with thermal effects in [7], the first paper about thermoelastic problems was discussed in [8]. In this paper, either adiabatic or isothermal condition is considered on the crack surface, the SIFs are extracted from the XFEM solution by an interaction integral, but it is only in isotropic materials. In [5], thermo-mechanical XFEM crack propagation analysis in functionally graded isotropic or orthotropic materials is dealt with. In [9], thermal and thermo-mechanical influence on crack propagation by extended meshless method is done. In [10], the thermal SIFs are obtained by crack closure integral or element-free Galerkin method. In [6, 9, 10], the material addressed is also limited to isotropic case, therefore, to my knowledge, for steady-state thermoelastic fracture problem in orthotropic medium using XFEM, few papers were reported in [5, 11].

In this paper, fracture analysis using XFEM in orthotropic thermoelastic problems is performed. The SIFs are extracted by interaction integral method. Several numerical examples are presented to validate the accuracy of results.

The outline of this paper is as follows. Section 2 recalls the fracture mechanics of orthotropic materials. Section 3 formulates the problem and introduces the discretization of the temperature field. In Section 4, the extraction of the SIFs from the XFEM solution is presented. It relies on interaction integrals in domain form with thermal effect. In Section 5, the method is illustrated by numerical examples and is compared with reference solutions. The conclusions are drawn in Section 6.

2 Fracture mechanics of orthotropic materials

The stress-strain relation [12] in linear elastic material can be written as

$$\varepsilon_\alpha = a_{\alpha\beta}\sigma_\beta, \quad (\alpha,\beta = 1,2,3), \tag{2.1}$$

with

$$\varepsilon_1 = \varepsilon_{11}, \quad \varepsilon_2 = \varepsilon_{22}, \quad \varepsilon_3 = \varepsilon_{33}, \quad \varepsilon_4 = 2\varepsilon_{23}, \quad \varepsilon_5 = 2\varepsilon_{31}, \quad \varepsilon_6 = 2\varepsilon_{12}, \tag{2.2a}$$

$$\sigma_1 = \sigma_{11}, \quad \sigma_2 = \sigma_{22}, \quad \sigma_3 = \sigma_{33}, \quad \sigma_4 = \sigma_{23}, \quad \sigma_5 = \sigma_{31}, \quad \sigma_6 = \sigma_{12}, \tag{2.2b}$$

where $a_{\alpha\beta}$ is components of orthotropic compliance tensor. Here, we assume the material is orthotropic with any types of loadings or general boundary conditions and a crack. Let (X_1, X_2) be global Cartesian co-ordinate, (x, y) be local Cartesian co-ordinate and (r, θ) be local polar co-ordinate defined on crack tip. As shown in Fig. 1.

The characteristic equation for orthotropic materials can be obtained using equilibrium and compatibility conditions [12]

$$a_{11}\mu^4 - 2a_{16}\mu^3 + (2a_{12} + a_{66})\mu^2 - 2a_{26}\mu + a_{22} = 0. \tag{2.3}$$

The roots of Eq. (2.3) are always either complex or purely imaginary in conjugate pairs as μ_1, $\bar{\mu_1}$ and μ_2, $\bar{\mu_2}$.

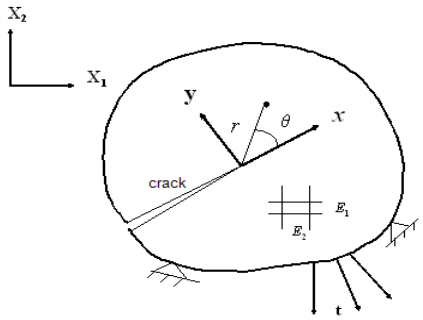

Figure 1: An arbitrary orthotropic body with traction t, with global Cartesian co-ordinate (X_1,X_2), local polar co-ordinate (r,θ) originating at the crack-tip and various boundary conditions.

Let $A_1=K_I/\sqrt{2\pi r}$, $A_2=K_{II}/\sqrt{2\pi r}$, $B_1=\sqrt{\cos\theta+\mu_1\sin\theta}$, $B_2=\sqrt{\cos\theta+\mu_2\sin\theta}$, then the near-tip asymptotic stress fields [13] for pure Mode I fracture can be written as

$$\sigma_{11}=A_1 Re\left[\frac{\mu_1\mu_2}{\mu_1-\mu_2}\left(\frac{\mu_2}{B_2}-\frac{\mu_1}{B_1}\right)\right], \tag{2.4a}$$

$$\sigma_{22}=A_1 Re\left[\frac{1}{\mu_1-\mu_2}\left(\frac{\mu_1}{B_2}-\frac{\mu_2}{B_1}\right)\right], \tag{2.4b}$$

$$\sigma_{12}=A_1 Re\left[\frac{\mu_1\mu_2}{\mu_1-\mu_2}\left(\frac{1}{B_1}-\frac{1}{B_2}\right)\right], \tag{2.4c}$$

and in the same way, for pure Mode II fracture, the stresses fields are [13]

$$\sigma_{11}=A_2 Re\left[\frac{1}{\mu_1-\mu_2}\left(\frac{\mu_2^2}{B_2}-\frac{\mu_1^2}{B_1}\right)\right], \tag{2.5a}$$

$$\sigma_{22}=A_2 Re\left[\frac{1}{\mu_1-\mu_2}\left(\frac{1}{B_2}-\frac{1}{B_1}\right)\right], \tag{2.5b}$$

$$\sigma_{12}=A_2 Re\left[\frac{1}{\mu_1-\mu_2}\left(\frac{\mu_1}{B_1}-\frac{\mu_2}{B_2}\right)\right]. \tag{2.5c}$$

3 Problem formulation and discretization

3.1 Governing equations

The 2D static linear orthotropic thermoelasticity equation in a domain Ω bounded by Γ are expressed as [8]

$$\mathbf{q}=-\mathbf{k}\nabla T\mathbf{k}=\begin{bmatrix} k_1 & 0 \\ 0 & k_2 \end{bmatrix}, \tag{3.1a}$$

$$-\mathbf{q}+\bar{Q}=0, \tag{3.1b}$$

$$\boldsymbol{\varepsilon} = \nabla_s \mathbf{u}, \tag{3.1c}$$

$$\boldsymbol{\varepsilon}_{\mathbf{T}} = \boldsymbol{\alpha}(T - T_0)\mathbf{I}\boldsymbol{\alpha} = \begin{bmatrix} \alpha_1 & 0 \\ 0 & \alpha_2 \end{bmatrix}, \tag{3.1d}$$

$$\boldsymbol{\sigma} = \mathbf{C} : (\boldsymbol{\varepsilon} - \boldsymbol{\varepsilon}_{\mathbf{T}}), \tag{3.1e}$$

$$\nabla \cdot \boldsymbol{\sigma} + \bar{\mathbf{b}} = \mathbf{0}, \tag{3.1f}$$

where, T is temperature, $\mathbf{q}$ heat flux, $\mathbf{u}$ displacement, $\boldsymbol{\varepsilon}$ strain tensor, $\boldsymbol{\sigma}$ stress tensor, $\boldsymbol{\varepsilon}_{\mathbf{T}}$ thermal expansion, T_0 reference temperature; the material properties are diffusivities in x,y directions $\mathbf{k}$, expansion coefficients in x,y directions $\boldsymbol{\alpha}$, and the orthotropic Hooke tensor $\mathbf{C}$; $\bar{Q}$ is heat source, and $\bar{\mathbf{b}}$ body force. $\mathbf{I}$ is the identity tensor and ∇_s is the symmetric gradient operator. The boundary conditions are listed below as

$$T = \bar{T} \qquad \text{on } \Gamma_T, \tag{3.2a}$$

$$\mathbf{q} \cdot n = \bar{\mathbf{q}} \qquad \text{on } \Gamma_q, \tag{3.2b}$$

$$\mathbf{u} = \bar{\mathbf{u}} \qquad \text{on } \Gamma_u, \tag{3.2c}$$

$$\boldsymbol{\sigma} \cdot \mathbf{n} = \bar{\mathbf{t}} \qquad \text{on } \Gamma_t, \tag{3.2d}$$

with $\Gamma_T \cup \Gamma_q = \Gamma_u \cup \Gamma_t = \Gamma$ and $\Gamma_T \cap \Gamma_q = \Gamma_u \cap \Gamma_t = \emptyset$. A crack Γ_c is present in Ω. It is assumed to be traction free ($\Gamma_c \subset \Gamma_t$, $\bar{\mathbf{t}} = \mathbf{0}$ on Γ_c). Here, we only focus on the case of an adiabatic crack ($\Gamma_c \subset \Gamma_q$, $\bar{q} = 0$ on Γ_c).

3.2 Adiabatic crack

In this case, the crack faces are adiabatic and also assumed to be traction free. The admissible displacement and temperature spaces can be written as

$$U = \{\mathbf{u} \in H_1^3(\Omega) : u = \bar{u} \text{ on } \Gamma_u \text{ and } u \text{ discontinuous on } \Gamma_c\}, \tag{3.3a}$$

$$\mathrm{Y} = \{\mathbf{u} \in H_1(\Omega) : T = \bar{T} \text{ on } \Gamma_T \text{ and } T \text{ discontinuous on } \Gamma_c\}. \tag{3.3b}$$

The weak form can be expressed as: Find $u \in U$ and $T \in \mathrm{Y}$ such that

$$\int_\Omega \boldsymbol{\varepsilon}(\mathbf{v}) : \mathbf{C} : \boldsymbol{\varepsilon}(\mathbf{u}) d\Omega = \int_\Omega \mathbf{v} \cdot \bar{\mathbf{b}} d\Omega + \int_{\Gamma_T} \mathbf{v} \cdot \bar{\mathbf{t}} d\Gamma + \int_\Omega \boldsymbol{\varepsilon}(\mathbf{v}) : \mathbf{C} : \boldsymbol{\varepsilon}_{\mathbf{T}} d\Omega, \tag{3.4a}$$

$$\int_\Omega \mathbf{q}(\mathbf{S}) \mathbf{k} \mathbf{q}(\mathbf{T}) d\Omega = -\int_\Omega S\bar{Q} d\Omega + \int_{\Gamma_q} S\bar{q} d\Gamma, \tag{3.4b}$$

are satisfied $\forall(\mathbf{v},\ \mathbf{S}) \in U_0 \times \mathrm{Y}_0$, where the subscript 0 denotes homogeneous essential conditions. Using XFEM, a standard local temperature or displacement approximation around the crack is enriched with jump function across the crack surfaces and the crack tip temperature or displacement enrichment function around crack tip. The same procedure is used for the thermoelastic in [8]. The shifted-XFEM [14, 15] enrichment formula-

tion for displacement components in the orthotropic material can be written as

$$\mathbf{u}(x,y)=\sum_{n\in N}N_n(x,y)\mathbf{a}_n+\sum_{n\in N_{cr}}N_n(x,y)[H(x,y)-H(x_n,y_n)]\mathbf{b}_n + \sum_{n\in N_{tip}}N_n(x,y)\sum_{m=1}^{M}[\mathbf{F}_m(r,\theta)-\mathbf{F}_m(r_n,\theta_n)]\mathbf{c}_{nm}, \tag{3.5}$$

where N_{cr} is the set of nodes whose support is crossed by the crack faces, while N_{tip} is the set of nodes inside a fixed area around the crack tip (geometry enrichment). The selection of enriched nodes (topological enrichment or geometry enrichment) for 2D crack problem is illustrated in Fig. 2 or Fig. 3. $\mathbf{a}_n$ is usual finite element nodal displacements, $\mathbf{b}_n$ and $\mathbf{c}_{nm}$ are enriched nodal displacement freedoms. $H(x,y)$ is the generalized Heaviside function which takes the value of $+1$ if (x,y) is above the crack surface and -1, otherwise. Here, $\{\mathbf{F}_m(r,\theta)\}_{m=1}^4$ are near tip asymptotic enrichment functions, which can be written as [14]

$$\{\mathbf{F}_m(r,\theta)\}_{m=1}^4=\left\{\sqrt{r}\cos\left(\frac{\theta_1}{2}\right)\sqrt{g_1(\theta)},\sqrt{r}\cos\left(\frac{\theta_2}{2}\right)\sqrt{g_2(\theta)}, \sqrt{r}\sin\left(\frac{\theta_1}{2}\right)\sqrt{g_1(\theta)},\sqrt{r}\sin\left(\frac{\theta_2}{2}\right)\sqrt{g_2(\theta)}\right\}, \tag{3.6}$$

where

$$g_j(\theta)=\sqrt{\cos^2(\theta)+\frac{\sin^2(\theta)}{p_j^2}},\quad j=1,2, \tag{3.7a}$$

$$\theta_j=\arctan\frac{y}{p_jx}=\arctan\frac{\tan\theta}{p_j}, \tag{3.7b}$$

$$p_1=\sqrt{A-\sqrt{A^2-\frac{C_{22}}{C_{11}}}},\quad p_2=\sqrt{A+\sqrt{A^2-\frac{C_{22}}{C_{11}}}},\quad A=\frac{1}{2}\times\left[\frac{C_{66}}{C_{11}}+\frac{C_{22}}{C_{66}}-\frac{(C_{12}+C_{66})^2}{C_{11}C_{66}}\right], \tag{3.7c}$$

where (r,θ) are polar co-ordinate with the origin defined at the crack-tip as defined in Fig. 1. C_{ij} $(i,j=1,2,6)$ are constitute coefficients. In this study, we assume that the crack faces are adiabatic, so the temperature is discontinuous across the crack faces and the heat flux is singular at the crack tip or crack front, the step function is $H(x,y)$, which is suitable to account for the temperature discontinuity.

Consequently, we discretize the temperature field in a way like the displacement field but using simply the third and the fourth branch functions in Eq. (3.6) (the choosing of enrichment terms is justified by the following Example 1), which are discontinuous branch functions [11]

$$T(x,y)=\sum_{n\in N}N_n(x,y)T_n+\sum_{n\in N_{cr}}N_n(x,y)[H(x,y)-H(x_n,y_n)]d_n + \sum_{n\in N_{tip}}N_n(x,y)\sum_{m=3}^{4}[\mathbf{F}_m(r,\theta)-\mathbf{F}(r_n,\theta_n)]e_{nm}. \tag{3.8}$$

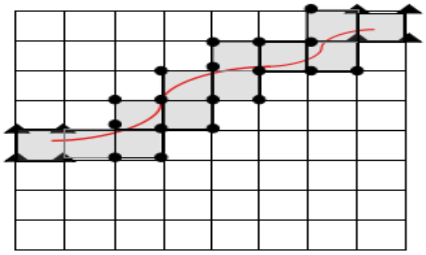

Figure 2: Selection of topological enriched nodes for 2D crack problem. Circled nodes (set of nodes N_{cr}) are enriched by the jump function whereas triangular nodes (set of nodes N_{tip}) are enriched by the crack tip branch functions. The gray elements are those cut by the crack.

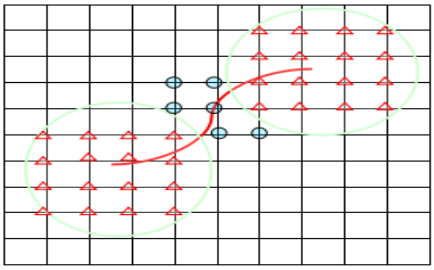

Figure 3: Fixing the near-tip enrichment scheme for selection of enriched nodes for 2D crack problem. Circled nodes (set of nodes N_{cr}) are enriched by the jump function whereas triangular nodes (set of nodes N_{tip}) are enriched by the crack tip branch functions.

4 SIFs calculations

The domain integral method for thermoelastic problem [16–18] is adopted for evaluating stress intensity factors in homogeneous orthotropic media. The standard path independent J-integral [19] for a cracked body is defined as

$$J=\lim_{\Gamma\to 0}\int_{\Gamma}(W\delta_{1j}-\sigma_{ij}u_{i,1})n_j d\Gamma, \tag{4.1}$$

where W is the strain energy density and n_j the component of the outward unit vector normal to an arbitrary contour Γ, as shown in Fig. 4, which surrounds the crack tip and encloses no other cracks. Here, we define a weight function q, which is a function varying from $q=1$ on crack tip to $q=0$ along the contour Γ, and arbitrary value but continuously changeable elsewhere within the domain enclosed by Γ. Then using the divergence theorem, the standard J-integral can be reduced into an equivalent domain form, given by

$$J=\int_A(\sigma_{ij}u_{i,1}-W\delta_{1j})q_{,j}dA+\int_A(\sigma_{ij}u_{i,1}-W\delta_{1j})_{,j}qdA. \tag{4.2}$$

Where A is the domain enclosed by Γ (shaded domain in Fig. 4).

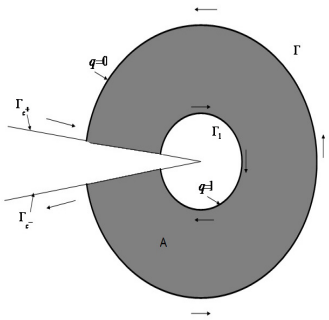

Figure 4: Area for domain integral.

For thermoelastic orthotropic material, the strain energy density can be written as

$$W=\frac{1}{2}\sigma_{ij}[\varepsilon_{ij}-\alpha_{ij}(T-T_0)], \tag{4.3}$$

while the constitutive equation is

$$\sigma_{ij}=D_{ijkl}[\varepsilon_{kl}-\alpha_{kl}(T-T_0)], \tag{4.4}$$

where D_{ijkl} is the components of constitutive tensor, α_{kl} the components of thermal expansion vector, T and T_0 are the absolute and reference temperature, respectively.

For the homogeneous orthotropic medium, Eq. (4.2) can be reduced into the classical domain form of thermal J-integral

$$J=\int_A(\sigma_{ij}u_{i,1}-W\delta_{1j})q_{,j}dA+\int_A(\sigma_{ij}\alpha_{ij}T_{,1})qdA. \tag{4.5}$$

By combining the actual and auxiliary solutions for obtaining the J-integral, one can write

$$J^{(1+2)}=J^{(1)}+J^{(2)}+I^{(1,2)}, \tag{4.6}$$

where $J^{(1+2)}$ is the J-integral value for the superposition state, $J^{(1)}$ and $J^{(2)}$ are J-integral value for actual and auxiliary states, respectively, and $I^{(1,2)}$ is the so-called interaction integral, which is given by

$$I^{(1,2)}=\int_A\left[(\sigma_{ij}^{(1)}u_{i,1}^{(2)}+\sigma_{ij}^{(2)}u_{i,1}^{(1)})-\frac{1}{2}(\sigma_{ij}^{(1)}\varepsilon_{ij}^{(2)}+\sigma_{ij}^{(2)}\varepsilon_{ij}^{*})\delta_{1j}\right]q_{,j}dA+\int_A[\sigma_{ij}^{(2)}\alpha_{ij}^{(1)}T_{,1}^{(1)}]qdA, \tag{4.7}$$

where $\varepsilon_{ij}^{*}=\varepsilon_{ij}^{(1)}-\alpha_{ij}^{(1)}(T^{(1)}-T_0^{(1)})$, superscript 1, 2 and 1+2 indicate fields and quantities associated with states 1, 2 and 1+2.

For elastic orthotropic solids under mixed-mode load conditions, the J-integral is just the energy release rate at the crack tip and is also related to SIFs as

$$J=\beta_{11}K_I^2+\beta_{12}K_IK_{II}+\beta_{22}K_{II}^2, \tag{4.8}$$

where

$$\beta_{11}=-\frac{a_{22}}{2}Im\left[\frac{\mu_1+\mu_2}{\mu_1\mu_2}\right],\quad \beta_{22}=\frac{a_{11}}{2}Im(\mu_1+\mu_2),\quad \beta_{12}=-\frac{a_{22}}{2}Im\left[\frac{1}{\mu_1\mu_2}\right]+\frac{a_{11}}{2}Im(\mu_1\mu_2).$$

Applying Eq. (4.8) to states 1, 2 and the superposed state 1+2 gives

$$J^{(1)}=\beta_{11}{K_I^1}^2+\beta_{12}K_I^1K_{II}^1+\beta_{22}{K_{II}^1}^2, \tag{4.9a}$$

$$J^{(2)}=\beta_{11}{K_I^2}^2+\beta_{12}K_I^2K_{II}^2+\beta_{22}{K_{II}^2}^2, \tag{4.9b}$$

$$I^{(1,2)}=2\beta_{11}K_I^1K_I^2+\beta_{12}(K_I^1K_{II}^2+K_I^2K_{II}^1)+2\beta_{22}K_{II}^1K_{II}^2. \tag{4.9c}$$

Let $K_I^2=1$ and $K_{II}^2=0$, Eq. (4.9c) reduces to

$$I^{(1,I)}=2\beta_{11}K_I^1+\beta_{12}K_{II}^1. \tag{4.10}$$

Similarly, let $K_I^2=0$ and $K_{II}^2=1$, Eq. (4.9c) reduces to

$$I^{(1,II)}=\beta_{12}K_I^1+2\beta_{22}K_{II}^1. \tag{4.11}$$

Hence, the mixed-mode SIFs (K_I^1 and K_{II}^1) can be obtained by solving a system of linear algebraic Eq. (4.10) and Eq. (4.11).

5 Numerical examples

In this section, the following examples are provided to assess the robustness of the proposed method. In all examples, plane stress condition is assumed. To improve the numerical accuracy, two layers of crack tip enrichment is used in the first or second examples, however, in third example, only one layer crack tip enrichment is used

(1) Homogeneous orthotropic plate with an inclined center crack under constant thermal strain.

(2) Inclined edge crack with several orientations of the axes of orthotropy under uniform heat flux.

(3) Plate with a central crack in special case (isotropy) of orthotropic thermoelasticity.

All three examples produce a pure Mode-II loading. The uncoupled orthotropic thermoelastic problem, the associated orthotropic temperature field problem is first solved by XFEM, the temperature field results so obtained are then used in subsequent XFEM numerical stress analysis. After stress analysis, the stress intensity factors in the crack tip are then obtained using domain form of interaction integral. Five different integral paths are used in J-integral, the resulting stress intensity factors are average value of five value obtained by five integral paths.

5.1 Example 1

This example presents an inclined center cracked homogeneous orthotropic plate, the geometry and boundary condition of the center crack are illustrated in Fig. 5. In [5], the author also neglect the effect of crack on the temperature fields, i.e., the mechanical fields are affected by the thermal response, while the thermal fields are not affected by the crack and mechanical fields. The material parameters of Young's modulus, Poisson's ratio and thermal expansion coefficient can be obtained from those special case in [5], i.e., in case of $\beta=\delta_1=\delta_2=0$, the orthotropic functionally material restores to homogeneous orthotropic material. $a/W=0.1$, $L/W=1.0$ and three crack inclined angles $\theta=0^\circ$,36° and 72° are considered here. The thermal boundary condition and corresponding equivalent mechanical load are shown in Fig. 5(a) and Fig. 5(b), respectively. The plane stress condition results in a uniform thermal strain when the crack is not considered.

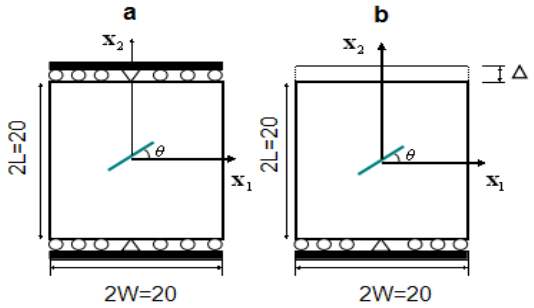

Figure 5: Inclined edge crack, (a) thermal-induced prescribed strain, and (b) mechanical loadings.

Table 1 presents the comparison of the normalized SIFs at the right crack tip using XFEM with those in [5] in terms of different crack inclined angles. It is shown that the results of good accordance is observed. This accordance also reflects the proposed example is a special case of that in [5] and the valid choosing of enrichment function in Eq. (3.8). In the FEM discretization, there are at least 182 nodes, 1504-node quadrilateral elements, as shown in Fig. 6(a). Fig. 6(b) shows the deformed mesh when $\alpha=15^\circ$.

Table 1: Normalized SIFs at the right crack tip.

crack angle (degree)	KI (XFEM)	KI (see [5])	KII (XFEM)	KII (see [5])
0	1.429	1.428	0.000	0.000
36	1.008	1.019	0.40	0.409
72	0.211	0.216	0.32	0.29

5.2 Example 2

For the second example (see [20]), as shown in Fig. 7, an adiabatic edge crack in the rectangular plate are considered, the dimensions of the plate is: W is width and its length

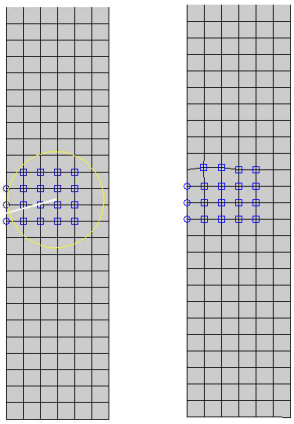

(a) (b)

Figure 6: Finite element mesh of edge crack with enriched nodes and circular J-integral contour around crack tip. (a) Finite element mesh of edge crack ($\alpha=15^\circ$) with enriched nodes and circular J-integral contour around crack tip. Circled nodes are enriched by the discontinuity function whereas squared nodes are enriched by the crack tip function, (b) deformed mesh edge crack ($\alpha=15^\circ$).

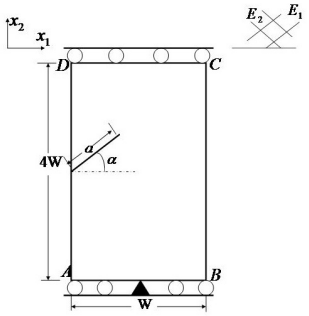

Figure 7: Inclined edge crack.

is taken to be four times its width, the two opposite ends, AB and CD, of the plate are assumed to be constrained in the x_2 direction and free to x_1 direction. The plate is subjected to a steady-state temperature load, the sides BC, AD and the crack surfaces are thermally insulated; the temperature of side AB is unchanged, but the side CD is cooled by temperature Θ_0. The plate material is glass/epoxy, the asterisks denoting values in directions of the principal material axes, the properties are those in [20].

In the present analysis, the range of inclined angle of the crack considered is 0° to 45°, and for each crack angle, the SIFs for relative crack lengths, $a=0.5$ is adopted. The results of SIFs are compared with those of boundary element method (BEM). The presented stress intensity factors are all being normalized by $K_0=E^*_{22}\alpha^*_{22}\Theta_0\sqrt{\pi a}$ [20].

Table 2 gives the comparison of the presented normalised stress intensity factors at the crack tip of the inclined edge crack obtained using XFEM and those obtained using BEM.

Table 2: Normalized SIFs-Example 2 for $a/W=0.5$.

crack angle (degree)	KI (XFEM)	KI (see [20])	% Diff	KII (XFEM)	KII (see [20])
0	0.628	0.643	2.33	0.000	-
15	0.620	0.622	0.32	0.06	0.060
30	0.543	0.554	1.99	0.096	0.133
45	0.423	0.470	10	0.161	0.179

The excellent accordance is obtained from the table. The relatively greater percentage discrepancies for K_{II}/K_0 can be attributed to their small magnitudes, which considerably decreases the accuracy of the results.

5.2.1 Influence of mesh refinement

The variation of the normalized SIFs K_I/K_0 with the mesh refinement using fixed near-tip enrichment domain scheme and topological enrichment scheme are shown in Fig. 8 and Fig. 9, respectively. Both scheme are in cases of $\alpha=0^\circ$ and $\alpha=15^\circ$.

Five different meshes are used with a normalized characteristic element length h/W varying between 0.15 and 0.015, we can see that most of the results are within 0.8% and compared to the topological enrichment scheme,the fixed near-tip enrichment domain

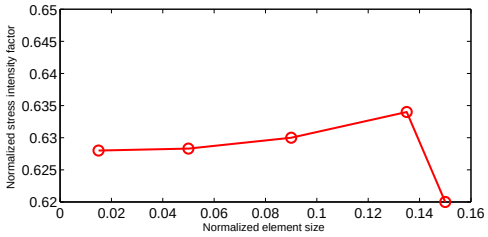

(a) Convergence of the K_I/K_0 for Example 2 in case of $\alpha=0^\circ$ using fixed near-tip enrichment domain scheme

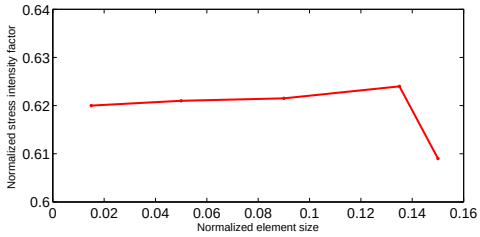

(b) Convergence of the K_I/K_0 for Example 2 in case of $\alpha=15^\circ$ using fixed near-tip enrichment domain scheme

Figure 8: Convergence of the K_I/K_0 for Example 2 using fixed near-tip enrichment domain scheme.

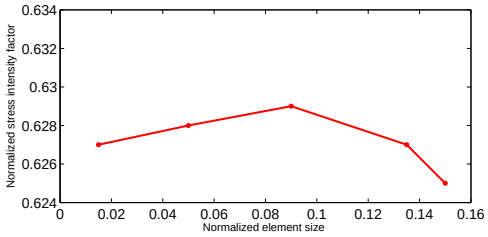

(a) Convergence of the K_I/K_0 for Example 2 in case of $\alpha=0^\circ$ using topological enrichment scheme

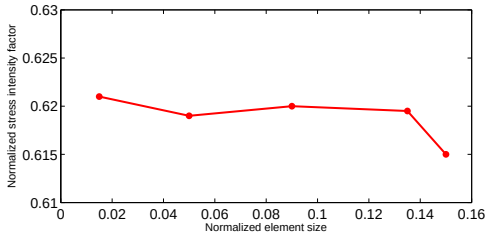

(b) Convergence of the K_I/K_0 for Example 2 in case of $\alpha=15^\circ$ using topological enrichment scheme

Figure 9: Convergence of the K_I/K_0 for Example 2 using topological enrichment scheme.

scheme improved the convergence of SIFs greatly.

5.2.2 Influence of Gauss quadrature

Due to the presence of enrichment term in XFEM, therefore the quadrature requires a higher order Gauss quadrature, the sub domain integration is adopted here, as shown in Fig. 10 (see [5]). A 3×3 Gauss quadrature is adopted in unenriched elements, a 5×5 Gauss quadrature is utilized for integration in elements containing Heaviside enriched node(s), and 7×7, 9×9, 11×11, 13×13 and 15×15 Gauss quadrature schemes are utilized for integration in elements containing crack tip enriched node(s).

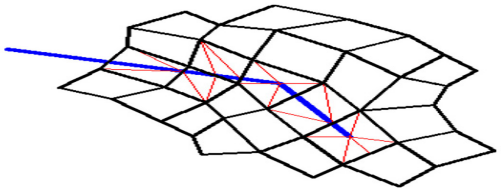

Figure 10: Integration sub domain around a crack.

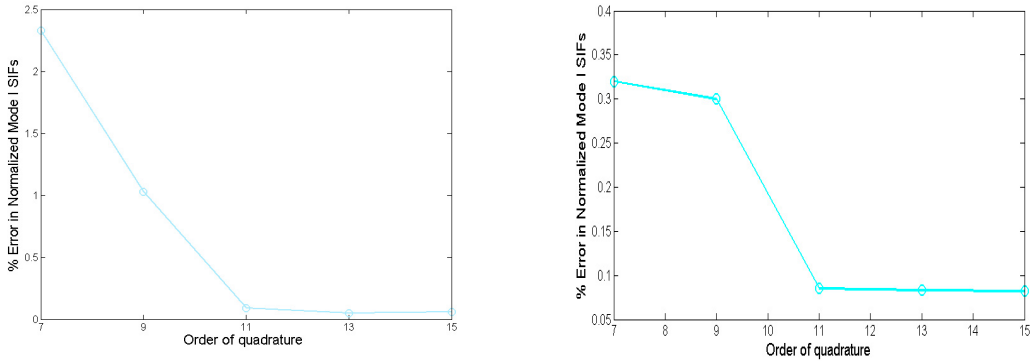

(a) Convergence of normalized Mode I SIFs with order of quadrature when $\alpha=0^\circ$

(b) Convergence of normalized Mode I SIFs with order of quadrature when $\alpha=15^\circ$

Figure 11: Convergence of normalized Mode I SIFs.

Fig. 11(a) and Fig. 11(b) present the convergence of normalized SIFs K_I/K_0 with increasing quadrature order for sub domain in cases of $\alpha=0^\circ$ and $\alpha=15^\circ$, respectively. When the quadrature order increases, the % error in normalized SIFs K_I/K_0 tends to zero. From these figures, it is shown that a high order ($>$11th order) of quadrature scheme is recommended around crack tip.

5.2.3 Influence of crack tip enrichments

In addition, to show the influence of crack tip enrichments on SIFs, Fig. 12 presents the comparison of normalized Mode II SIFs with and without orthotropic crack tip enrich-

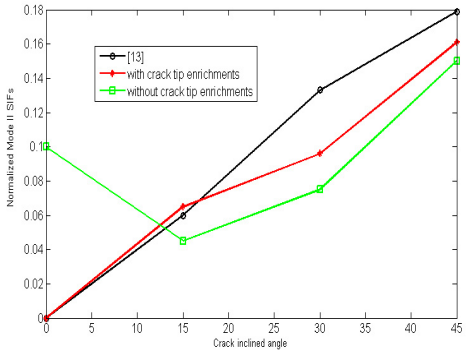

Figure 12: Comparison of normalized Mode II SIFs with and without orthotropic crack tip enrichments in cases of $\alpha=0°$,15°,30° and 45°.

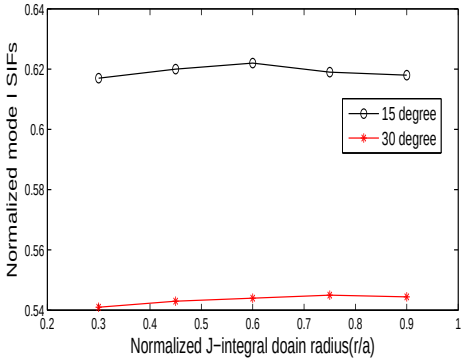

Figure 13: Normalized Mode I SIFs versus radius of J-integral domain in cases of $\alpha=15°$ and 30°.

ments in cases of $\alpha=0°$,15°,30° and 45°. From Fig. 12, we can see that the results using orthotropic crack tip enrichments agrees quite well with the reference solution, however, without using crack tip enrichment, the results dramatically deviate from the reference solution.

5.2.4 Influence of radius of the J-integral domain

In order to study the influence of radius of the J-integral domain on SIFs, five different J-integral contour paths with normalized domain radius of $r/a=0.3,0.45,0.6,0.75$ and 0.9 are adopted, as depicted in Fig. 13, which presents Normalized Mode I SIFs versus radius of J-integral domain in cases of $\alpha=15°$ and 30°, from this figure, it is obvious that the radius of J-integral domain does not has notably influence on the SIFs.

5.3 Example 3

A rectangular plate of width $2W$ and length $2L$ and a central crack of length $2a$ is shown in Fig. 14. This configuration with $L/W=1.0$ and a/W varying from 0.1 to 0.6 is solved for

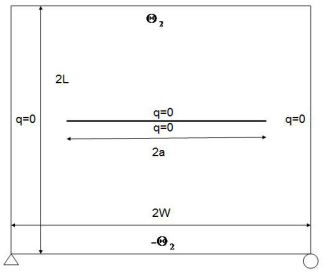

Figure 14: Plate with a central crack.

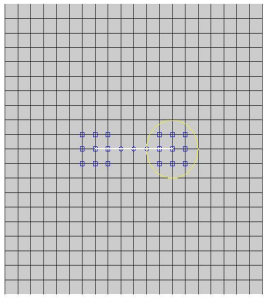

Figure 15: Finite element mesh of central crack with enriched nodes and circular J-integral contour around crack tip. Circled nodes are enriched by the discontinuity function whereas squared nodes are enriched by the crack tip functions.

adiabatic pure Mode II condition. The example have the following material properties used in [21]: $E_1 = E_2 = 2.184\times10^{11}$Pa, Poisson's ratio v_{12}; and the coefficients of linear expansion α_1,α_2=$1.67\times10^{-5}per^{\circ}$C, in x,y directions. Results are regardless of the thermal conductivities k_1, k_2, here, $k_1 = k_2$. The finite element mesh with enriched nodes and circular J-integral contour around crack tip is shown in Fig. 15, in the mesh, there are 400 square elements, 441 nodes, to model the isotropy, $\mu_1 = 0.99i$, $\mu_1 = 1.01i$ in characteristic Eq. (2.4a) is assumed. The resulting SIFs are normalized by $K_0 = \alpha_1\Theta_2 E(W)^{0.5}$. In Table 3, the SIFs are compared with those reported in the handbook [1], and those reported in [22] obtained by a dual boundary element method. The results are in close agreement.

Table 3: Normalized SIFs-Example 3.

a/W	This study	see [22]	see [1]
0.1	0.020	0.018	0.021
0.2	0.055	0.054	0.053
0.3	0.096	0.095	0.094
0.4	0.142	0.141	0.141
0.5	0.192	0.190	0.188
0.6	0.248	0.243	0.247

6 Conclusions

The XFEM was applied to the analysis of steady-state orthotropic thermoelastic problems in cracked structures. The temperature is discretized similarly to the common XFEM discretization of the displacement field. A domain-independent interaction integral which is applied to orthotropic material is used to extract the SIFs from the thermomechanical XFEM solution.Numerical examples are presented to validate the accuracy of the proposed method.

Acknowledgments

This work was supported by the National Natural Science Foundation of China (No. 11471262).

References

[1] Y. MURAKAMI AND L. KEER, *Stress intensity factors handbook,* J. Appl. Mech., 60 (1993), pp. 1063.
[2] T. BELYTSCHKO AND T. BLACK, *Elastic crack growth in finite elements with minimal remeshing,* Int. J. Numer. Meth. Eng., 45 (1999), pp. 601–620.
[3] S. BORDAS, P. V. NGUYEN, C. DUNANT, A. GUIDOUM AND H. NGUYEN-DANG, *An extended finite element library,* Int. J. Numer. Meth. Eng., 71 (2007), pp. 703–732.
[4] R. MERLE AND J. DOLBOW, *Solving thermal and phase change problems with the extended finite element method,* Comput. Mech., 28 (2002), pp. 339–350.
[5] S. HOSSEINI, H. BAYESTEH AND S. MOHAMMADI, *Thermo-mechanical xfem crack propagation analysis of functionally graded materials,* Mat. Sci. Eng. A, 561 (2013), pp. 285–302.
[6] M. ROKHI AND M. SHARIATI, *Coupled thermoelasticity of a functionally graded cracked layer under thermomechanical shocks,* Arch. Mech., 65 (2013), pp. 71–96.
[7] P. AREIAS AND T. BELYTSCHKO, *Two-scale method for shear bands: thermal effects and variable bandwidth,* Int. J. Numer. Meth. Eng., 72 (2007), pp. 658–696.
[8] M. DUFLOT, *The extended finite element method in thermoelastic fracture mechanics,* Int. J. Numer. Meth. Eng., 74 (2008), pp. 827–847.
[9] L. BOUHALA, A. MAKRADI AND S. BELOUETTAR, *Thermal and thermo-mechanical influence on crack propagation using an extended mesh free method,* Eng. Fract. Mech., 88 (2012), pp. 35–48.
[10] N. MUTHU, S. MAITI, B. FALZON AND I. GUIAMATSIA, *A comparison of stress intensity factors obtained through crack closure integral and other approaches using extended element-free galerkin method*, Comput. Mech., 52 (2013), pp. 587–605.
[11] A. ZAMANI AND M. R. ESLAMI, *Implementation of the extended finite element method for dynamic thermoelastic fracture initiation,* Int. J. Solids. Struct., 47 (2010), pp. 1392–1404.
[12] S. LEKHNITSKII, Theory of Elasticity of an Anisotropic Elastic Body, Hoden-Day, San Francisco, 1965.
[13] G. C. SIH, P. PARIS AND G. IRWIN, *On cracks in rectilinearly anisotropic bodies,* Int. J. Fract. Mech., 1 (1965), pp. 189–203.

[14] A. ASADPOURE AND S. MOHAMMADI, *Developing new enrichment functions for crack simulation in orthotropic media by the extended finite element method,* Int. J. Numer. Meth. Eng., 69 (2007), pp. 2150–2172.
[15] M. J. PAIS, Variable Amplitude Fatigue Analysis Using Surrogate Models and Exact XFEM Reanalysis, PhD thesis, University of Florida, 2011.
[16] J. CHEN, *Determination of thermal stress intensity factors for an interface crack in a graded orthotropic coating-substrate structure,* Int. J. Fracture, 133 (2005), pp. 303–328.
[17] J. H. KIM AND G. H. PAULINO, *The interaction integral for fracture of orthotropic functionally graded materials: evaluation of stress intensity factors,* Int. J. Solids. Struct, 40 (2003), pp. 3967–4001.
[18] A. KC AND J. H. KIM, *Interaction integrals for thermal fracture of functionally graded materials,* Eng. Fract. Mech., 75 (2008), pp. 2542–2565.
[19] J. R. RICE, *A path independent integral and the approximate analysis of strain concentration by notches and cracks,* J. Appl. Mech., 35 (1968), pp. 379–386.
[20] Y. SHIAH AND C. TAN, *Fracture mechanics analysis in 2-d anisotropic thermoelasticity using bem,* Comput. Model. Eng., 1 (2000), pp. 91–99.
[21] S. H. EBRAHIMI, S. MOHAMMADI AND A. ASADPOURE, *An extended finite element (XFEM) approach for crack analysis in composite media,* Int. J. Civ. Eng., 6 (2008), pp. 198–207.
[22] N. PRASAD, M. ALIABADI AND D. ROOKE, *The dual boundary element method for thermoelastic crack problems,* Int. J. Fracture, 66 (1994), pp. 255–272.